

A New Consideration on Tendon-Tension Control System of Robot Hands

Makoto Kaneko*, Mitsuo Wada**, Hitoshi Maekawa***, Kazuo Tanie***

* Kyushu Inst. of Technology
Iizuka, Fukuoka 820 JAPAN

** Industrial Products Res. Inst., MITI
Tsukuba, Ibaraki 305 JAPAN

*** Mech. Eng. Lab., MITI
Tsukuba, Ibaraki 305 JAPAN

Abstract

This paper discusses force control for the tendon-sheath driving system typically used to actuate robotic finger joints. For a simple tendon-sheath model, the transmission characteristics were first formulated with the newly introduced factors *apparent tendon-stiffness* and *equivalent backlash*. An interesting aspect is that *apparent tendon-stiffness* changes when the tendon is pulled or loosened, while tendon-stiffness itself keeps constant under the absence of friction. This unexpected behavior is confirmed by simulations as well as experiments. The authors also consider the effect of apparent tendon-stiffness on force control and show that the direction-dependent behavior of *apparent tendon-stiffness* eventually brings about a *direction-dependent response* in the force control system without carefully designed control strategy.

1. Introduction

There are many works discussing robot hands, such as grasp planning [1]-[4], stable grasps [5]-[10], finger tip sensors [11]-[12]. With a small size and insufficient space to mount actuators inside the fingers, the finger actuators are normally placed on the forearm of the manipulator and the power is transmitted from an actuator to a finger joint through either a tendon-pulley driving system [13], [14] or a tendon-sheath driving system [15]-[18]. With its simple transmission mechanism and very flexible power transmission route, we focus on the tendon-sheath driving system in this study. This transmission system, however, includes nonlinear characteristics due to tendon-compliance together with friction between the tendon and sheath, and sometimes causes unexpected behaviors in force servo systems. For example, it has been reported in Salisbury-HAND [19] and Darmstadt-HAND [20] that the stability of the force servo system depends on input due to such nonlinear characteristics. To clarify these phenomena and implement a suitable force control strategy, it is essential to fully understand the transmission characteristics of the tendon-sheath driving system.

Okada [21] first employed a theoretical approach toward the transmission characteristics of the tendon-sheath system during the development of the Okada-HAND. He has discussed the effect of friction on the transmission characteristics caused by the tendon-sheath interaction, but has not taken tendon-compliance into consideration. Townsend and Salisbury [19] have considered the stability of the torque servo system using a simple model composed of a small mass placed over a frictional plane with two springs connected to the mass.

The starting point of this paper is to clarify the nature of the transmission characteristics of the tendon-sheath driving system for a simple model incorporating both compliance and friction. Through our analysis, we first introduce a non-dimensional

parameter λ representing friction force, and then formulate the transmission characteristics as a function of λ with the newly defined *apparent tendon-stiffness* and *equivalent backlash*. We demonstrate an interesting characteristic of *apparent tendon-stiffness*, namely, that the strength of the stiffness changes as whether the tendon is pulled or loosened. The existence of *apparent tendon-stiffness* is verified by simulation using more general model and also by experiments. From the viewpoint of force feedback control, the *apparent tendon-stiffness* plays an important role in determining the response of the force control system, because it directly influences the loop gain of the system. We show that the direction-dependent behavior of *apparent tendon-stiffness* brings about a *direction-dependent response* for force control system. We also show that equivalent backlash is proportional to tendon-pretension as well as non-dimensional parameter λ , and thus, a large pretension makes the system nonlinearity increase and brings about another nonlinear effect on the system.

2. Transmission characteristics of tendon-sheath system

Figure 1 shows a force control system including single tendon-sheath transmission system and actuator driving system, where T , ξ , R , k_e , and k_s are tendon-tension, tendon-displacement, tendon radius of curvature, environment stiffness, and sensor stiffness, respectively, and subscripts "in" and "out" denote the input side and the output side, respectively. Although a finger joint is normally driven by two tendons connected a joint pulley, we purposely focus on a single tendon-sheath system as shown in Fig.1. Because we can reduce the boundary conditions appearing at both ends of the tendons without losing the true behavior of the transmission system. In this chapter, we discuss the transmission characteristics of tendon-sheath system which is surrounded by alternate long and short dotted line in Fig.1.

2.1 Analytical approach for a simple model

In this section, we consider the effects of friction and compliance. For simplicity, we assume that both tendon-curvature and tendon-pretension are uniform along the length of the tendon. This simple model still exhibits the basic behavior of the tendon-sheath driving system when input signal changes slow enough to ensure that any dynamic effects are suppressed.

We begin by discussing the friction which exists in the tendon-sheath driving system. There are basically two kinds of friction in the system. One is tension-dependent friction caused by curving the tendon under arbitrary pretension. The other is tension-independent friction caused only by contact between the tendon and sheath irrespective of tendon-tension. With a simple experiment, we can confirm that tension-dependent friction is

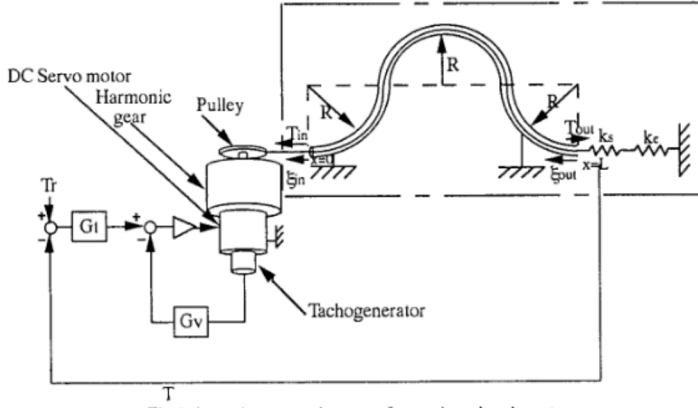


Fig.1 A tension control system for tendon-sheath system

much larger than tension-independent friction, thus enabling us to ignore the tension-independent friction.

Figure 2 shows the force balance for a small tendon element with a curvature, where F and N are the friction force and normal force, respectively from the sheath. The relation of $N = \mu F$ gives $F = \mu N = \mu T dy$, where $dy = dx/R$ and μ is a frictional coefficient which changes according to whether tendon is moving or not, and given by,

$$\mu = \begin{cases} \mu_s & (\xi = 0) \\ \mu_d & (\xi \neq 0) \end{cases} \quad (1)$$

Combining the force balance equation with Hook's law, we obtain a vector equation in the following form,

$$\frac{d\Phi}{dx} = D\Phi - \rho\Lambda \quad (2)$$

where $\Phi = [T, \delta]^T$, $\Lambda = [0, T_0]^T$, $\rho = 1/EA$, and,

$$D = \begin{bmatrix} -\frac{\mu}{R} sgn\xi & 0 \\ \rho & 0 \end{bmatrix} \quad (3)$$

$$sgn\xi = \begin{cases} 1 & (\xi \geq 0) \\ -1 & (\xi < 0) \end{cases} \quad (4)$$

where δ , E , A , T_0 , and μ are tendon elongation from $x=0$ to $x=\delta$, Young's modulus, cross sectional area of tendon, tendon-pretension, and frictional coefficient, respectively. The solution of eq. (2) is given by,

$$T(x) = \begin{cases} T_{in} \exp(-\frac{\mu}{R} x sgn\xi) & (x < L_1) \\ T_0 & (x \geq L_1) \end{cases} \quad (5)$$

$$\delta(x) = \begin{cases} [H(x) - T_0 x + \frac{R}{\mu} T_{in} sgn\xi] \rho & (x < L_1) \\ [H(L_1) - T_0 L_1 + \frac{R}{\mu} T_{in} sgn\xi] \rho & (x \geq L_1) \end{cases} \quad (6)$$

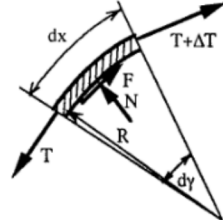


Fig.2 Force balance for small tendon-element with curvature

$$H(x) = -\frac{R}{\mu} T_{in} sgn\xi \exp(-\frac{\mu}{R} L_1 sgn\xi) \quad (7)$$

In eq. (5) and (6), L_1 is the length automatically determined in the following way. For an input-tension change from T_0 to T_{in} , a tension-change appears only between $x=0$ and $x=L_1$ according to the strength of input-tension, while tendon-tension does not change in $x > L_1$. Thus, L_1 satisfies the following condition.

$$L_1 = \min\{x \in T(x)=T_0\} \quad (8)$$

Equation (5) is a well-known formula expressing tension distribution along the tendon-length [15], [16], while eq.(6) has not yet been introduced. Now, let us consider the case in which input-tension increases gradually. During this movement, L_1 continuously increases, and eventually, L_1 coincides with L . This means that the tension-change at the input side is transmitted to the other end by the deformation and movement of the small tendon-element. This condition is given by

$$T_0 = T_{in} \exp(-\frac{\mu}{R} L sgn\xi) \quad (9)$$

$$d(L) = [\frac{R}{\mu} T_{in} sgn\xi \exp(-\frac{\mu}{R} L sgn\xi) - T_0 L + \frac{R}{\mu} T_{in} sgn\xi] \rho \quad (10)$$

In other words, tendon-tension at the output side does not change until the input displacement exceeds $d(L)$. We can, therefore, regard $d(L)$ as a kind of backlash for the tendon-sheath driving system, and thus, we define *effective backlash* ξ_B in the following form.

$$\begin{aligned} \xi_B &= \{d(L)\}_{T_0=T_{in}\exp(\lambda)} \\ &= \frac{T_0 L}{EA} \frac{\exp(\lambda) - 1}{\lambda} \end{aligned} \quad (11)$$

$$\lambda = \frac{\mu L sgn\xi}{R} \quad (12)$$

λ is a non-dimensional parameter and indicates the total friction force acting on the tendon under unit tendon-tension. λ reduces to zero when $\mu \rightarrow 0$ or $R \rightarrow \infty$ or $L \rightarrow 0$.

$$\frac{\exp(\lambda) - \lambda - 1}{\lambda} = \sum_{n=1}^{\infty} \frac{1}{(n+1)!} \lambda^n \quad (13)$$

Therefore, ξ_B reduces to zero with $\lambda \rightarrow 0$, as expected. There is another possibility that ξ_B reduces to zero, namely, it corresponds to zero-pretension. Since equivalent backlash is proportional to tendon-pretension, eq. (11) also explains the experimental results that Vossoughi and Donath pointed out in their studies [16]. We would note also that the sign of ξ_B depends on that of λ . Now, we will consider the tendon behavior when the operating point is moving outside the equivalent backlash region. This means that $|\xi_{in}|$ is greater than $|\xi_B|$. In this case, the boundary conditions at the output side are written by

$$\xi_{out} + \{\delta(L)\}_{T_{in}=T_{out}} \exp(\lambda) = \xi_{in} \quad (14)$$

$$T_{out} - T_0 = k_{se} \xi_{out} \quad (1/k_{se} = 1/k_e + 1/k_s) \quad (15)$$

From eq. (5), (6), (14), and (15) we obtain the transmission characteristics with surprisingly simple form.

$$T_{out} - T_0 = K_t (\xi_{in} - \xi_B) \quad (16)$$

where

$$\cdot \frac{1}{K_t} = \frac{1}{k_e} + \frac{1}{k_s} + \frac{1}{K_{ap}} \quad (17)$$

$$K_{ap} = K_w \frac{\lambda}{\exp(\lambda) - 1} \quad (18)$$

$$K_w = \frac{EA}{L} \quad (19)$$

This form is especially convenient for discussing the basic behavior of the force (or tension) control system, because eq. (16) is the direct expression of the transmission characteristics for the tendon-sheath driving system composed of an actuator generating ξ_{in} and a tension sensor detecting T_{out} . Further details on the relationship between eq. (16) and system behavior will be discussed in the following chapter. At this point, we note that except the *equivalent backlash*, the obtained transmission characteristic is quite similar to Hook's law prescribing the linear relationship between applied force and displacement for an elastic body. Also the tendon in sheath behaves as if it were a spring with a variable spring constant, that is, the original stiffness K_w apparently shifts according to eq. (18) under friction. Hereafter we will call K_{ap} *apparent tendon-stiffness*. Although authors have pointed out the existence of a virtual spring within the backlash region for the tendon-sheath driving system [20], apparent tendon-stiffness is essentially different from that appearing in the backlash region, $\lambda/\{\exp(\lambda)-1\}$ prescribing the shifted value from K_w is rewritten by

$$\frac{\lambda}{\exp(\lambda) - 1} = \frac{1}{1 + \sum_{n=1}^{\infty} \frac{\lambda^n}{(n+1)!}} \quad (20)$$

Therefore, $\lambda/\{\exp(\lambda)-1\} < 1$ while tendon is pulled ($\lambda > 0$), and $\lambda/\{\exp(\lambda)-1\} > 1$ while tendon is loosened ($\lambda < 0$). Assuming that K_{ap1} and K_{ap2} are *apparent tendon-stiffnesses* in the pulling phase and in the loosening phase, respectively, eq.(20) suggests $K_{ap1} < K_w < K_{ap2}$. Since $K_{ap} \rightarrow K_w$ and $\xi_B \rightarrow 0$ with $\lambda \rightarrow 0$, eq.(16) exactly coincides with Hook's law under the absence of frictional effects. Therefore, we can take eq.(16) as an extended Hook's law which is applicable for the tendon-sheath system.

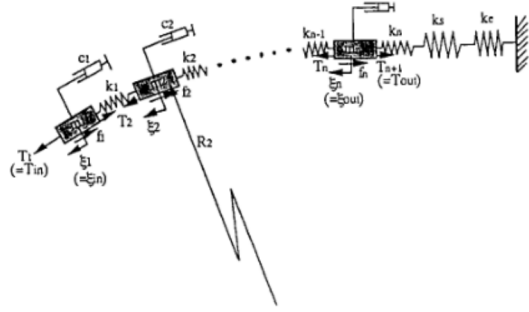


Fig.3 Simulation model

These analytical results give us fundamental knowledge on transmission characteristics of the tendon-sheath system, and help us to understand both simulation results and experimental results.

2.2 Numerical approach for a generalized model

In this section, we explore the transmission characteristics numerically for a more generalized model, considering tendon-mass and damping in addition to tendon-stiffness. Figure 3 shows the simulation model, where m_i , c_i , R_i , and k_i are respectively mass of i -th tendon-element, damping coefficient of i -th tendon-element, radius of curvature i -th tendon-element, and spring constant of the spring connecting between i -th tendon-element and $i+1$ th tendon-element. The equation of motion of this system is expressed by,

$$M\ddot{z} + C\dot{z} = DT \quad (21)$$

where $M = \text{diag}(m_1, m_2, \dots, m_n)$, $C = \text{diag}(c_1, c_2, \dots, c_n)$, $z = [\xi_1, \xi_2, \dots, \xi_n]^T$, $T = [T_1, T_2, \dots, T_n]^T$. Matrix $D \in \mathbb{R}^{nx(n+1)}$ is given by,

$$D = \begin{bmatrix} 1 - \text{sgn} \xi_1 \langle \mu_1 \rangle \Delta L / R_1 & -1 & 0 & \dots & 0 \\ 0 & 1 - \text{sgn} \xi_2 \langle \mu_2 \rangle \Delta L / R_2 & -1 & 0 & \dots & 0 \\ \dots & \dots & \dots & \dots & \dots & \dots \\ 0 & \dots & 0 & 1 - \text{sgn} \xi_n \langle \mu_n \rangle \Delta L / R_n & -1 & \dots \end{bmatrix} \quad (22)$$

where $\langle \mu_i \rangle$ is the friction coefficient between i -th tendon-element and sheath, and the rule of $\langle x \rangle$ is based on eq. (1). The relationship between tendon-tension and tendon deformation for each tendon-element is collected in vector form.

$$T = Kz + T_k \quad (23)$$

where $T_k = [T_1, T_2, \dots, T_0]^T \in \mathbb{R}^{n+1}$ is a known vector composing of input tendon-tension T_1 and tendon-pretension T_0 . The matrix $K \in \mathbb{R}^{(n+1) \times n}$ is written as,

$$K = \begin{bmatrix} 0 & \dots & \dots & 0 \\ k_1 & -k_1 & 0 & \dots & 0 \\ 0 & k_2 & -k_2 & 0 & \dots & 0 \\ \dots & \dots & \dots & \dots & \dots & \dots \\ 0 & \dots & 0 & k_{n-1} & -k_{n-1} & 0 \\ 0 & \dots & 0 & 0 & k'_n & 0 \end{bmatrix} \quad (24)$$

where $1/k_n = 1/k_n + 1/k_e + 1/k_s$. Substituting eq. (23) into eq. (21) yields,

$$\ddot{z} + M^{-1}C\ddot{z} = M^{-1}D(Kz + T_k) \quad (25)$$

Equation (25) can be solved numerically using a difference form. In simulations, tendon-tension at the input side is given as a sinusoidal function of time t .

$$\begin{aligned} T_{in} &= T_I \\ &= T_m \sin \omega t + T_0 \end{aligned} \quad (26)$$

where T_m is the amplitude of tendon-tension and is never greater than T_0 because the tendon driving system only works under positive tendon-tension.

Figure 4 shows simulation results, where k_e and k_s are assumed to be infinitely large. To check the simulation program, we begin by examining the input-output relationships under the condition that the angular velocity ω of the sinusoidal function for input tendon-tension is small enough frequency to suppress any dynamic effect. Figure 4 (a) shows simulation results obtained under $f=0.04$ Hz, where $\mu_{si}=\mu_{di}=0.1$ ($i=1, 2, \dots, n$). Although μ_{si} is essentially different from μ_{di} , the condition of $\mu_{si}=\mu_{di}$ is purposely set to compare with analytical results. The dotted lines in Fig.4(a) show analytical solutions introduced in the previous section where $v=\xi_{in}/L/R$. The non-dimensional parameter v is more convenient than λ because it does not contain $\text{sgn}(d\xi/dt)$. The dotted line in the middle corresponds to theoretical values when friction is ignored. Without friction, the simulation result coincides exactly with this line, although it is not shown here. From Fig.4 (a), we can confirm that, except for the backlash region, the operating point moves along the slope of the *apparent tendon-stiffness* which is obtained by analysis for the simple models. Thus, the developed simulation program must be valid as far as the dynamic effects are not involved.

Figure 4 (b) and (c) are simulation results with $f=0.5$ Hz and 5.0 Hz, respectively under different frictional coefficients, namely, $\mu_{si}=0.3$ and $\mu_{di}=0.1$. In case of frequency $f=0.5$ (Hz), the operating points partly shift from the analytical solutions which are valid when all tendon elements move along the slope of *apparent tendon-stiffness*. The distinct shifts especially appear around the switching points from the backlash region to outside backlash region. In this particular region, a part of tendon moves, while the rest part is not. Thus, static friction force will coexist with dynamic friction force in the same tendon-sheath, will bring about a complicated behavior of operating point. The shifts from the analytical solutions may be due to these reasons. Such a distinct shift disappears when the frequency increases to 5 Hz. Although some differences between analytical results and simulation results are recognized, the analytical results for the simple model provide fairly essential transmission characteristics of the tendon-sheath system as far as *apparent tendon-stiffness* is concerned.

2.3 Experimental approach

Figure 5 shows the experimental result when sinusoidal force input is imparted to the input side of the tendon with a frequency of 0.4 Hz, where Fig.5 (a) and Fig.5 (b) are transmission characteristics for $T_{in}-T_{out}$ and $\xi_{in}-T_{out}$, respectively. The experimental results for $T_{in}-T_{out}$ closely agree with the simulation results and eventually with the analytical results. With the exception of $\xi_{in}<0.5$ (mm), the experimental results for ξ_{in} -

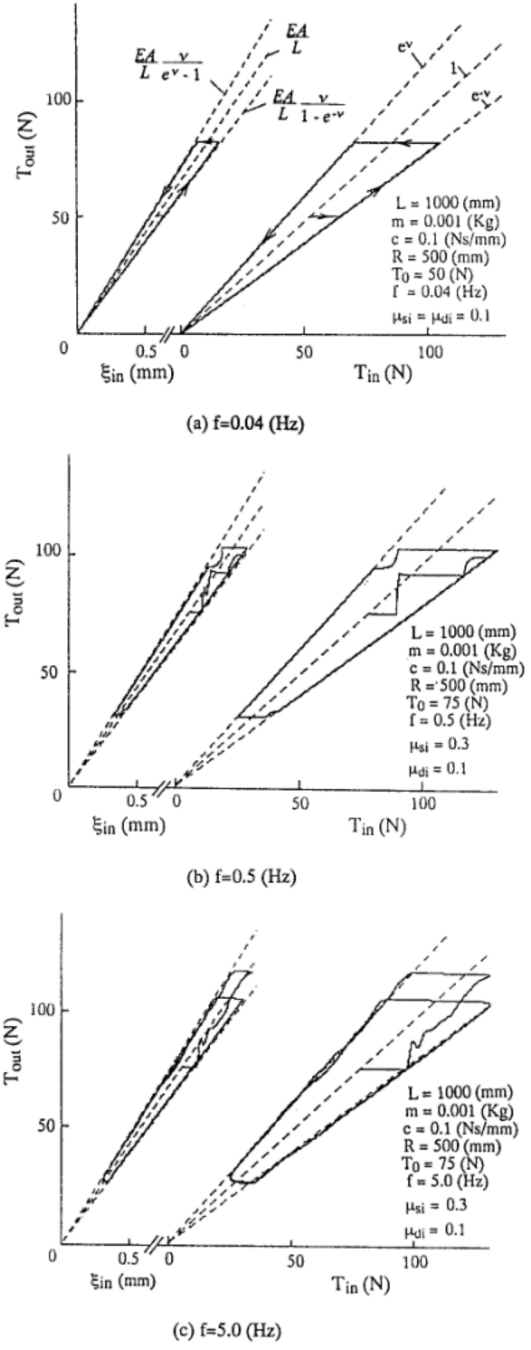


Fig.4 Simulation results

T_{out} also fairly agree with those obtained theoretically. The different behavior of $\xi_{in}<0.5$ (mm) may be due to tension-independent friction which is not considered here. The most

important result obtained through these experiments is that we could confirm the existence of *apparent tendon-stiffness* in the relationship between ξ_{in} and T_{out} .

3. Nonlinearities and force control system

Another objective in this paper is to explore the influence of nonlinearities, that is, *apparent tendon-stiffness* and *equivalent backlash* on such a force (or tension) control system.

3.1 Effect of Apparent tendon-stiffness

We will again consider a force servo system with apparent tendon-stiffness as shown in Fig. 1. We assume that the actuation system is composed of a DC servo motor and a high reduction gear such as harmonic drive gear. This assumption enables us to make the feedback torque from the gear output shaft to the motor rotor negligible, whereas this feedback torque is significant in a Direct Drive system. Also assuming the transmission characteristic of tendon-sheath expressed by eq. (16), we can combine the equation of motion outside the equivalent backlash region with simple control law, and write in the following form,

$$J_m \ddot{\theta} + G_v \dot{\theta} = G_t r \{ T_r - K_t (\xi_{in} - \xi_B) \} \quad (27)$$

where T_r , J_m , G_v , r , and θ are reference tension, effective inertia of actuator, force forward gain, velocity feedback gain, and actuator angular displacement. The relation of $\xi = r\theta$ gives,

$$J_m \ddot{\theta} + G_v \dot{\theta} = G_t r T_r - G_t K_t r^2 (\theta - \theta_B) \quad (28)$$

where $r\theta_B = \xi_B$. With $T_r=0$, $x_1=\theta$, and $x_2=d\theta/dt$, eq. (28) may be written

$$\dot{x}_1 = x_2 \quad (29)$$

$$\dot{x}_2 = -2\xi \omega_1 x_2 - \omega_1^2 (x_1 - \theta_B) \quad (30)$$

giving

$$\frac{\dot{x}_2}{\dot{x}_1} = \frac{-2\xi \omega_1 x_2 - \omega_1^2 (x_1 - \theta_B)}{x_2} \quad (31)$$

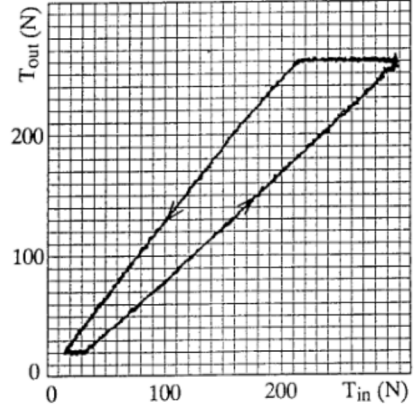
where

$$\omega_1^2 = \frac{K_t G_t r^2}{J_m} \quad (32)$$

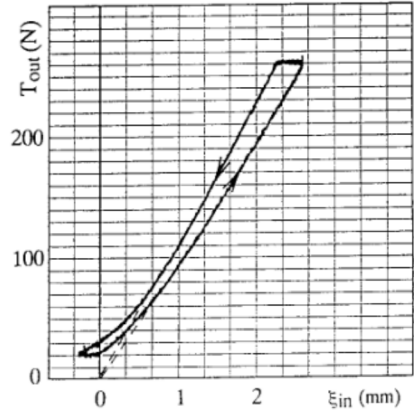
$$\xi = \frac{G_v}{2r} \sqrt{\frac{J_m}{K_t G_t}} \quad (33)$$

From eq. (11), (17), and (18), ζ , ω_1 , and θ_B are functions of x_2 . We will now formulate the motion in the equivalent backlash region. The tendon-tension at the output side does not change when $d\theta/dt$ reverse until θ has moved through the equivalent backlash, a distance of $\theta_B(+)|\theta_B(-)|$. If θ_0 is the value of θ when $x_2=0$ then during the motion of the actuator shaft through the equivalent backlash the output position θ remains at $\theta_0-\theta_B'$ where θ_B' is the equivalent backlash based on the velocity $d\theta/dt$ before reversing. Assuming that ω_1 and ζ do not change between the two regions, we obtain,

$$\frac{\dot{x}_2}{\dot{x}_1} = \frac{-2\xi \omega_1 x_2 - \omega_1^2 (\theta_0 - \theta_B')}{x_2} \quad (34)$$



(a) Transmission characteristics between T_{in} and T_{out}



(b) Transmission characteristics between ξ_{in} and T_{out}

To explain the influence of *apparent tendon-stiffness* on a force servo system using an example, we assume that the step response from $T-\Delta T$ to T exhibits critical damping behavior. With this assumption, the operating point moves along the right-side slope of K_t including *apparent tendon-stiffness* K_{ap} with $\lambda>0$ and reaches the equilibrium point without overshooting. Next, let us consider the step response from $T+\Delta T$ to T . In this case, the operating point moves along the left-side slope of K_t including *apparent tendon-tension* K_{ap} with $\lambda<0$. Now, we define ζ_1 and ζ_2 , where ζ_1 and ζ_2 are equivalent damping coefficients when operating points move along the right-side slope and the left-side slope, respectively. Since $K_{aph}>0 < K_{apl}<0$, $\zeta_2 < \zeta_1 = 1$. Thus, the operating point never stops at the equilibrium point without overshooting in the case of a step response from $T+\Delta T$ to T . We also see these behaviors in phase plane as shown in Fig.6, where lines (I) and (II) correspond to the responses for $T-\Delta T \rightarrow T$ and $T+\Delta T \rightarrow T$, respectively, and backlash motion appears between a and b. The important feature is that the behavior in $x_2>0$ is different from that of $x_2<0$ because of *apparent tendon-stiffness*. For example, $dx_2/dt=0$ gives

$$x_2 = \frac{\omega_1}{2\zeta} (x_1 - \theta_B) \quad (35)$$

From eq. (32) and (33), $\omega_1/(2\zeta) = G_l K_t r^2 / (J_m G_v)$. Since $K_{ap} \lambda > 0$ $< K_{ap} \lambda < 0$,

$$\left| \frac{\omega_1}{2\zeta} \right|_{\lambda>0} < \left| \frac{\omega_1}{2\zeta} \right|_{\lambda<0} \quad (36)$$

As shown in Fig.6, inequality (36) gives us two lines with different slopes leading to $dx_2/dt=0$ for $x_2>0$ and $x_2<0$, while those are same in the well-known backlash characteristics appeared in the gears situated between motor shaft and load shaft. These different slopes bring about different responses between the pulling phase and the loosening phase as shown in Fig.6. These considerations suggest that there exists a *direction-dependent response* for a force control system with a tendon-sheath driving system.

Figure 7 is an experimental result showing the force step responses for six different steps $0 \rightarrow T_{r1} \rightarrow T_{r2} \rightarrow T_{r3} \rightarrow T_{r2} \rightarrow T_{r1} \rightarrow 0$, where $T_{r1}=60(N)$, $T_{r2}=40(N)$, and $T_{r3}=20(N)$. In Fig.7, the response in $T_{r3} \rightarrow T_{r2}$ exhibits overshooting behavior, while the response in $T_{r1} \rightarrow T_{r2}$ show overdamping behavior. This direction-dependent response comes from the characteristics of *apparent tendon-stiffness* with different strengths depending on the direction the operating point moves.

3.2 Effect on equivalent backlash

A servo system involving a large equivalent backlash causes unstable behavior with a stable limit cycle. During oscillation, the amplitude is proportional to equivalent backlash [20]. From the viewpoint of reducing the magnitude of oscillation, equivalent backlash should be designed to be small. From eq.(11), there are three possibilities for reducing equivalent backlash. One approach is to reduce tendon-pretension, another is to use a tendon with large diameter to increase cross-sectional area of tendon. And one other is to reduce non-dimensional parameter, which may be difficult to achieve without sacrificing the flexibility acquired by using the tendon-sheath driving system.

4. Conclusion

From the viewpoint of executing force control for a tendon-sheath driving system used to actuate robotic hands, the transmission characteristics of the system were first analyzed for a simple model. Through this analysis, we showed that the input-output relationship can be expressed in linear form with the newly introduced *equivalent backlash* and *apparent tendon-stiffness*. The existence of both *equivalent backlash* and *apparent tendon-stiffness* were confirmed not only by simulation but also by experiment. We showed that apparent tendon-stiffness changes depending on whether tendon is pulled or loosened, eventually, causing a direction-dependent response for force control. We also explored the effect of equivalent backlash on force control.

references:

- [1] Park, Y., and G. Starr, Optimal grasping using a multifingered robot hand, Proc. of IEEE Int. Conf. on Robotics and Automation, 689, 1990.
- [2] Omata, T., Fingertip positions of a multifingered hands, Proc. of IEEE Int. Conf. on Robotics and Automation, 1562, 1990.
- [3] Kaneko, M. and K. Tanie, Contact point detection for grasping of an Unknown object using self-posture changeability (SPC), Proc. of IEEE Int. Conf. on Robotics and Automation, 864, 1990.
- [4] Kaneko, M. and K. Tanie, Contact point detection for grasping of an unknown object using joint compliance, Proc. of IEEE Int. Workshop on Intelligent Robots and Systems '90, 845, 1990.
- [5] Hanafusa, H. and H. Asada, Stable prehension by a robot hand with elastic fingers, Proc. of 7th Int. Symp. on Industrial Robots, Tokyo, 361, 1977.
- [6] Salisbury, J.K., Kinematic and force analysis of articulated hands, Ph.D. Thesis, Dept. of Mechanical Engineering, Stanford University, May 1982.
- [7] Cutkosky, M.R. and P.K. Wright, Friction , stability and the design of robotic fingers, Int. Journal of Robotics Research, vol.5, no.4, 20-37, 1986.
- [8] Nguyen, V., Constructing stable grasps in 3D, Proc. of IEEE Int. Conf. on Robotics and Automation, Raleigh, 234-239, 1987.
- [9] Fearing, R.S., Simplified grasping and manipulation with dexterous robot hands, IEEE journal of Robotics and Automation, vol.2, no.4, 188-195, 1986.
- [10] Fukuda, T., N. Kitamura, and K. Tanie, Adaptive force control of manipulators with consideration of object dynamics, Proc. of IEEE Int. Conf. on Robotics and Automation, 1543, 1987.
- [11] Dario P., and G. Buttazzo, An anthropomorphic robot finger for investigating artificial tactile perception, Int J. Robotics Research, vol.6, no.3, 25-48, 1987.
- [12] Cutkosky, M.R. and R.D.Howe, Dynamic tactile sensing. In Romany '88:7th CISM-IFToMM Symp. on the Theory and Practice of Robots and Manipulators, Udine, Italy, 1988.
- [13] Kaneko, M., K. Yokoi, and K. Tanie, On a new torque sensor for tendon drive fingers, IEEE Trans. on Robotics and Automation, vol.6, no.4, 501, 1990.
- [14] Jacobsen, S. C., E. K. Iversen, D. F. Knutti, R. T. Johnson, and K. B. Biggers, Design of the Utah/M.I.T. dexterous hand, Proc. of IEEE Int. Conf. on Robotics and Automation, San Francisco, 1520-1532, 1986.
- [15] Okada, T., Object-handling system for manual industry, IEEE Trans. Sys., Man, and Cybern., Vol. SMC-9-2, 79, 1979.
- [16] Vossoughi, R. and M. Donath, Robot hand impedance control in the presence of mechanical nonlinearities, ASME PED-Vol. 115, 67, 1985.
- [17] Sugano, S., H. Suzuki, O. Matsumoto, S. Mutoh, and I. Kato, Consideration of velocity terms in finger-arm coordination motion planning, Preprint of Symp. on Robot Control, Karlsruhe, 7.1-7.6, 1988.
- [18] Paetsch, W. and M. Kaneko, A three fingered, multijointed gripper for experimental use, Proc. of IEEE Int. Workshop on Intelligent Robots and Systems, 853, 1990.
- [19] Townsend, W. T. and J. K. Salisbury, The effect of Coulomb friction and stick-slip on force control, Proc. of IEEE Int. Conf. on Robotics and Automation, Raleigh, 240-245, 1987.
- [20] Kaneko, M., W. Paetsch, G. Kegel, and H. Tolle, Input-dependent stability on joint torque control of robot hands, Proc. of IEEE Int. Conf. on Robotics and Automation, 1057, 1990.
- [21] Okada, T., Force control of an artificial finger driven by a hose-guided wire, Trans. SICE, Vol. 14, No. 2, 155. (in Japanese), 1976.

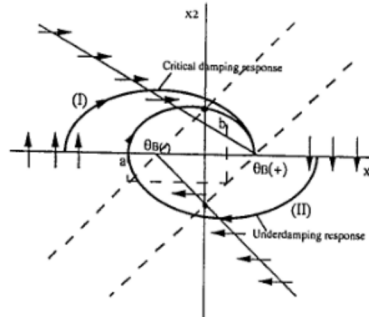


Fig.6 Trajectories of operating point in phase plane

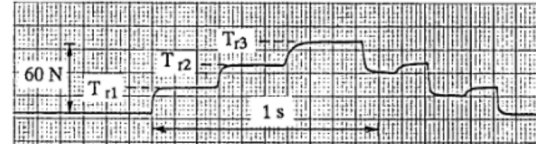


Fig. 7 Force step responses ($G_l=7.0$, $G_v=2.0$)